physica status solidi a
www.pss-a.com

Electronic and Topological Analysis for New Phases of Chromium Nitride

Marco Marín-Suárez, Leidy L. Alzate-Vargas, Jorge David, Mauricio Arroyave-Franco, and Mario E. Vélez*

Chromium nitride (CrN) in its NaCl-type phase has been widely studied through density functional theory (DFT) in order to analyze its electronic properties. By the means of DFT with the Becke's three parameter Lee-Yang-Parr (B3LYP) hybrid functional, the same stoichiometry is studied in two unreported hypothetical phases in addition to the nonsynthesized and previously reported zinc-blende-type phase. The cohesive energy of every structure is calculated, and the analysis of this quantity indicated that all crystals are stable and that there is an unreported phase more stable than the synthesized one. The calculated electronic dispersion relation and density of electronic states allowed for the determination that these three phases have a conducting behavior. The symmetry of some bands is determined as a result of the crystal field splitting for chromium *d* states. The topology of the electron density was studied in order to determine its properties at bond critical points (BCPs). The form of the Laplacian of the density and its gradient trajectories allowed to locate ring critical points in these structures. From these calculations, it is concluded that all three phases are ionic crystals. The synthesized NaCl-type phase is studied in order to compare and confirm the results.

1. Introduction

Chromium nitride (CrN) is a material of high technological and industrial importance. Due to its resistance to corrosion and oxidation,[1,2] high hardness, low electrical resistance, and high melting point,[3] it is used as a coating material[4,5] in magnetic storage devices and superconductors[6–9] and as a selective solar absorber. At room temperature, CrN is a paramagnetic material[10] with an *fcc* crystal structure,[11] while at temperatures below Néel Temperature (276–283 K) the crystal structure is in an orthorhombic antiferromagnetic phase (AFM) with a space group *Pnma*.[12] In addition molecular dynamics calculations by Shulumba et al.[13] were done and allowed the determination of the transition temperature in good agreement with experimentation.

M. Marín-Suárez, L. L. Alzate-Vargas, Dr. J. David,
Prof. M. Arroyave-Franco, Prof. M. E. Vélez
Departamento de Ciencias Físicas, Escuela de Ciencias, Universidad EAFIT A.A. 1226, Medellín, Colombia
E-mail: mmarins@eafit.edu.co

DOI: 10.1002/pssa.201700576

Due to its widespread applications, structural, electronic, and elastic properties of this material have been widely studied both experimentally and through ab initio techniques. Rivadulla et al.[14] developed a new method to synthesize CrN by ammonolysis of Cr_3S_4 and measured its bulk modulus. They reported that cubic CrN has a high bulk modulus (340–430 GPa), comparable to that of known hard materials, they also developed calculations on this phase and found a reduction of this bulk modulus at high pressures. But this assertion was put into debate by Alling et al. given the method to simulate the paramagnetic behavior of cubic CrN.[15] Zhang and Gall[16] performed an experimental analysis of the electronic properties of cubic CrN and vibrational modes suggesting that it is a Mott-Hubbard-type insulator with a small to negligible indirect band gap. Similar calculations carried by Zhou and collaborators, concluded that ferromagnetic and antiferromagnetic cubic CrN are (meta)stable phases, while a nonmagnetic arrangement is neither mechanically nor dynamically stable also determined the transition temperature between paramagnet and antiferromagnet to be 293 K.[17]

Other studies have made calculations of the electronic structure. Herwadkar and Lambrecht[10] calculated it using the local spin-density approximation corrected by Hubbard Coulomb terms for *d* electrons (LSDA + *U*), and Botana et al.[18] using different potentials. In search of new structures, studies about hypothetical solid phases of many materials have been made.[19] Concerning CrN crystal structures, Antonov and Iordanova[20] found three new crystal structures described by the space groups *P*4/*mmm*, *I*4/*mmm*, and *Pmnm* using density functional theory (DFT) with the gradient generalized approximation (GGA) of Perdew, Burke, and Ernzerhof (PBE), and Perdew and Wang (PW). Eck and collaborators[6] also have made DFT calculations of the zinc-blende-type structure of CrN with space group symmetry $F\bar{4}3m$ and found a conducting behavior of this phase, as did Miao and Lambrecht,[21] who in addition determined a ferromagnetic ordering in this phase.

Liang et al.[9] performed electronic structure calculations using DFT in order to analyze the magnetostructural transition of the paramagnetic cubic phase into the antiferromagnetic orthorhombic phase. They concluded that the interplay between

structural distortions and spin degrees of freedom is responsible for structural changes which agrees with the explanation given by Filippetti et al.[22] who show that the orthorhombic AFM (in the [100] plane) phase is the most stable among other possible magnetic arrangements. Filippetti and Hill[23] also explained how and why this interplay is present in CrN through DFT calculations, concluding that the stress anisotropy caused by the magnetic force for this transition is the responsible. In spite of these conclusions Alling et al.[24] showed that as the CrN is a highly correlated material an LSDA + U analysis and further is needed in order to understand this structural transition. Brik and Ma[25] estimated the band structure and density of states (DOS), using GGA and local density approximation (LDA) and concluded that CrN has a strong nonlocalization of the d states of Cr and $2p$ states of N, indicating the importance of the hybridization of orbitals in the description of mechanical properties.

This contribution reports calculations of first principles based on DFT. The main goal is to examine new hypothetical crystallographic configurations of CrN in order to analyze the electronic behavior by calculating the electronic band structure, the DOS for each crystal, and the electronic density (ρ) and its Laplacian. The last quantities are to be calculated in order to characterize the bonding types in the studied phases following the theory of atoms in molecules (QTAIM) by Bader, which gives a strict definition of bonds in crystals.[26–29] Studies about CrN have been used in past reports in order to analyze magnetic ordering. However, the present report does not have that intention; its main goal is to make an electronic characterization of new hypothetical phases of this material.

2. Methods

2.1. Computational Details

The CRYSTAL09[30,31] software was used to optimize and characterize the crystal structures generated by an evolutionary algorithm implemented in USPEX.[32–34] Geometry optimization was carried out by using analytical energy gradients with respect to the atomic coordinates and the unit cell parameters for each crystal structure.

All electron ab intio DFT[35–37] calculations were performed using a hybrid DFT-HF (Hartree-Fock) exchange-correlation functional B3LYP (Becke's three-parameter Lee-Yang-Parr),[38–40] as implemented in the CRYSTAL09 code. All ab initio calculations were performed using Mike Towler Gaussian basis sets.[41] Gaussian basis sets 86-411d41G and 7-311G were used for chromium and nitrogen, respectively. Gaussian basis sets have been used since they have been successfully applied to all-electron calculations.[19,31] Also all calculations were made simulating standard pressure and temperature conditions (299 K and 101 325 Pa), so every stability and electronic structure report is under these conditions.

As stated in the previous section, researches about CrN always consider net magnetic moments of Cr atoms in order to predict correctly its structure. In this work spin-polarized calculations were made in order to consider different spins with different densities, and so net magnetic moments can be find on the Cr atoms that allows to simulate a magnetic structure, which has shown to be important in these type of calculations although no magnetic order has been imposed. Here we only show the spin-majority bands and DOS while the bonding contour plots contain the total electronic density.

In order to avoid spurious interactions between the diffuse functions and the core functions of neighbor atoms, a diffuse exponential sp for nitrogen ($\alpha = 0.113$) was eliminated. Brillouin Zone integration was performed on a Pack-Monkhorst **k**-mesh[42] of $12 \times 12 \times 12$. This mesh was chosen because of the convergence of the energy value with this meshing for every structure analyzed. Also it showed an agreement between the calculations and experimental data[11] of the lattice parameter of the NaCl-type structure. This can be seen since the error is always ≈1.8% (the experimental datum is $a = 4.0718$ Å).

The CRYSTAL09 package was used to perform all calculations. The calculation of band structures (in the vicinity of Fermi's level) of all four considered structures was made choosing the **k**-path according to Ref. [43]. The Bilbao Crystallographic database[44] was used to obtain the irreducible representations (irreps) for each **k**-vector and their compatibility relations by using the COMPATIBILITY RELATIONS program. The TOPOND program[45] was used to obtain the critical points for each crystal and the Laplacian contour plots. The search of critical points was made in the asymmetric unit of the crystal through an eigenvector-following algorithm, which runs during ten steps with 10 neighbors for each point in a radius of 10 Å. These processes were performed within a box defined in the intervals $[0; 1] \times [0; 1] \times [0; 1]$ with a discretization step of 0.025 in each direction. No further constraints were applied. To improve the calculations, these were focused on the bond critical point.

2.2. Studied Phases

This study introduces two new crystallographic structures in addition to an experimentally reported one and another theoretically reported. Experimental data indicates that CrN crystallizes in a NaCl-type structure[11] at room temperature. The lattice parameters of the $Fm\bar{3}m$ structure calculated in this work match those of Ref. [11] with an error of ≈1.8%.

In addition, the reported zinc-blende-type structure is studied and its calculated lattice parameter match the one reported in Ref. [6] with a 0.86% difference. The crystallographic properties and cohesive energy (E_{coh}, in eV/atom) of each phase are shown in **Table 1**. In order to calculate the cohesive energy, the following formula was used:

$$E_{coh} = \frac{1}{2}\left(E_{Tot}^{CrN} - E_{Tot}^{Cr} - E_{Tot}^{N}\right), \quad (1)$$

where E_{Tot}^{Cr}, E_{Tot}^{N}, and E_{Tot}^{CrN} are the total energy of a chromium atom, a nitrogen atom and the crystal structure of CrN. Atomic positions, Wyckoff positions and site symmetries are shown in **Table 2** to complement the structural information of each solid.

Structure Model 1 is a C-centered orthorhombic phase with the *Cmcm* space group, with four atoms per unit cell (two of chromium and two of nitrogen). Each atom of Cr is in a site with point group C_{2h}, coordinated by six N atoms forming a triangular

Table 1. Cohesive energies (in eV atom^{-1}) and lattice parameters (in Å) for the CrN crystal structures. SM: Structure Model, SG: space group.

SM	SG	E_{coh}	Lattice parameters		
			a	b	c
1	$Cmcm$	−7.19	2.7304	4.7263	5.1354
2	$Fm\bar{3}m$	−6.84	4.0770	–	–
			4.1480[a]	–	–
3	$F\bar{4}3m$	−6.79	4.3371	–	–
			4.3000[b]	–	–
4	$Pmmm$	−5.76	3.1782	6.5639	2.7618

[a] Reported in Ref. [11]; [b] reported in Ref. [6].

antiprism. The N atoms are located in positions with symmetry point group C_{2v}, with six Cr atoms as first-nearest neighbors arranged in a triangular prism form. Structure Model 4 is a simple orthorhombic structure that belongs to the $Pmmm$ space group, having four atoms per unit cell (two of Cr and two of N). The Cr and N atoms have coordination of two and are in sites with C_{2v} symmetry group. Neither of these structures adopt a particular structure prototype.

Structure Model 2 is a face-centered cubic with the $Fm\bar{3}m$ symmetry group, which has two atoms per unit cell (one of Cr and one of N). Cr atoms are placed in points with site symmetry group O_h, octahedrally coordinated by six N atoms which are also octahedrally coordinated by six Cr atoms. Structure Model 3 is also a face-centered cubic, but with the $F\bar{4}3m$ space group and having two atoms per unit cells (one of Cr and one of N). In this structure, each Cr is placed in a site with point group T_d, tetrahedrally coordinated by four N atoms. These atoms are in equivalent positions. The conventional cells of each studied phase are shown in **Figure 1**.

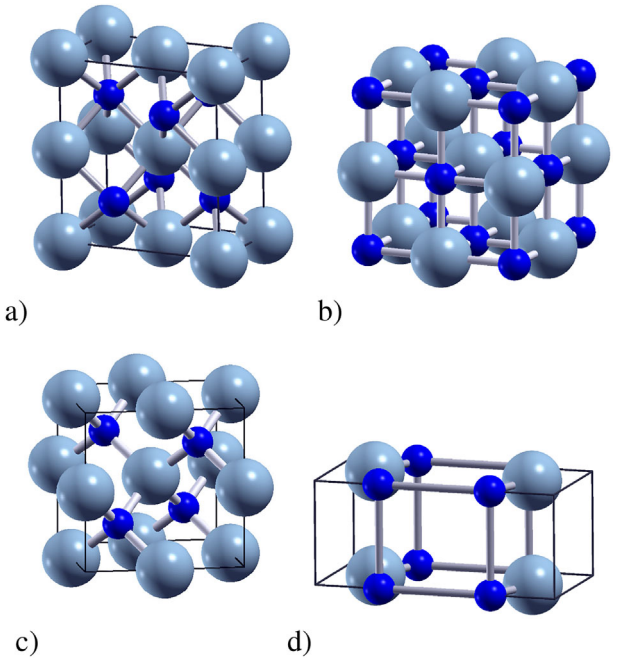

Figure 1. Conventional cells of CrN for (a) Structure Model 1, (b) Structure Model 2, (c) Structure Model 3, and (d) Structure Model 4. Big balls represent chromium atoms and small balls represent nitrogen atoms. Images obtained with XCrySDen.[46]

3. Results and Discussion

3.1. Crystal Energies

In order to estimate the thermodynamic stability of CrN crystals, the cohesive energies were calculated. This is the energy necessary to dissociate the solid into separated atoms or ions.[47] Thus, negative values mean that the structure is thermodynamically stable. The cohesive energies of each crystal are shown in Table 1. As can be seen, all E_{coh} are negative, hence all structures are thermodynamically stable. From this table, it can be seen that Structure Model 1 is the most stable while Structure Model 4 is the least. It is interesting to note that Structure Model 1 is more stable than the usually reported Structure Model 2 by only 0.35 eV and than Structure Model 3 by 0.40 eV and has a lower E_{coh} by ≈1.00 eV than that of Structure Model 4. It seems strange that one of the hypothetical phases is more stable than the synthesized one. Since it has been more easily found, one would expect it to be more stable at standard pressure and temperature conditions that all other hypothetical phases, but here the opposite has been found. Further studies about the hypothetical Structure Model 1 should be done with different methods of calculations in order to confirm the value of E_{coh}. Also the dynamic stability of these structure remains to be confirmed by means of the calculation of its phonon dispersion relation, so the reason that Structure Model 1 has not been experimentally found yet could be because is not dynamically stable. Also consider that

Table 2. Wyckoff positions, symmetries and atomic positions of the Cr and N atoms. SM: Structure Model.

SM	Cr			N		
	Wyckoff position	Symmetry	Atomic position	Wyckoff position	Symmetry	Atomic position
1	4a	$2/m(C_{2h})$	(0, 0, 0)	4c	$m2m(C_{2v})$	$\left(-\frac{1}{2}, -\frac{4}{25}, \frac{1}{4}\right)$
2	4b	$m\bar{3}m(O_h)$	$\left(\frac{1}{2}, \frac{1}{2}, \frac{1}{2}\right)$	4a	$m\bar{3}m(O_h)$	(0, 0, 0)
3	4b	$\bar{4}3m(T_d)$	$\left(\frac{1}{2}, \frac{1}{2}, \frac{1}{2}\right)$	4c	$\bar{4}3m(T_d)$	$\left(\frac{1}{4}, \frac{1}{4}, \frac{1}{4}\right)$
4	2o	$m2m(C_{2v})$	$\left(-\frac{1}{2}, -\frac{17}{100}, 0\right)$	2m	$m2m(C_{2v})$	$\left(0, \frac{27}{100}, 0\right)$

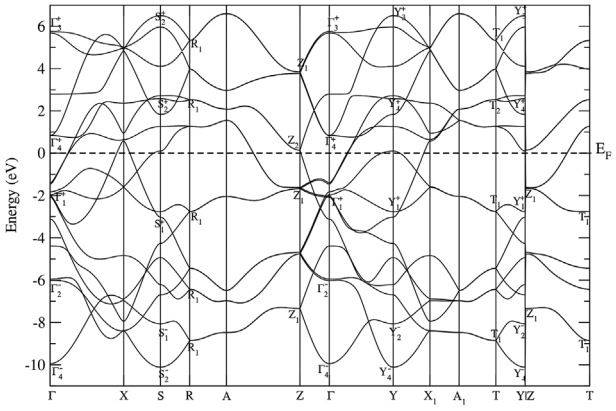

Figure 2. Calculated dispersion relation for Structure Model 1. The dispersion relation is labeled as follows: for Γ, S, and Y points all the subindexes denote 1-dimensional representations. For the R, Z, and T positions, all the subindexes represent 2-dimensional irreps.

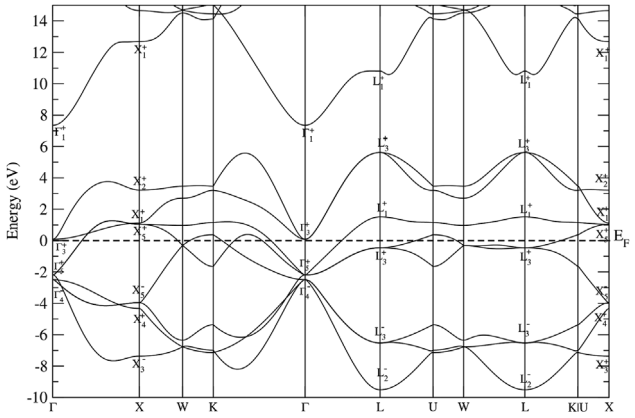

Figure 4. Calculated dispersion relation for Structure Model 2. The dispersion relation is labeled as follows: for the Γ point, the subindex 1 denotes a 1-dimensional irrep, 3 denotes a 2-dimensional irrep, and 4 and 5 denotes a 3-dimensional irrep. For the L point, subindexes 1 and 2 denote 1-dimensional irreps, and 3 denotes 2-dimensional irreps. For the X point, subindexes 1, 2, 3 and 4 refer to 1-dimensional irreps, and 5 refers to a 2-dimensional irrep.

the difference between E_{coh} for Structure Models 1 and 2 is less than 0.5 eV and this could be a computational error.

3.2. Electronic Structure

The calculated dispersion relation, total, and partial DOS for Cr and N atoms in all crystals are shown in Figure 2–9. For dispersion relations and DOS, the energy has been shifted so that Fermi energy is at 0 eV.

3.2.1. Structure Model 1

Figure 2 shows the electronic dispersion relation around the Fermi level (E_F). Since there are bands crossing this level, Structure Model 1 is an electric conductor. This figure displays a region starting in its lowest energy point at Y position with the D_{2h} symmetry point group, this point has the Y_4^- 1-dimensional irrep. The highest energy position of this region is at the same **k**-point but has the Y_3^+ 1-dimensional irrep. The energy width of the region between Y_4^- and Y_3^+ is ≈16.70 eV.

In **Figure 3**, the total and projected DOS in the *d*-type orbitals of Cr and *sp*-type orbitals of N in the same range of the dispersion relation is shown. It is evident from the total DOS that there are states at E_F, thus, we are dealing with an electric conductor, confirming the information contained in Figure 2. Furthermore the total DOS seems to be a local maximum at E_F which could lead to instabilities or to majority-minority spin splitting in the case of CrN, this supports the fact that further studies about stability remain to be done. In all projected DOS plots, only the contributions of *d*-type orbitals from Cr and *sp*-type orbitals from N are shown, since those contributions are dominant in all structure models.

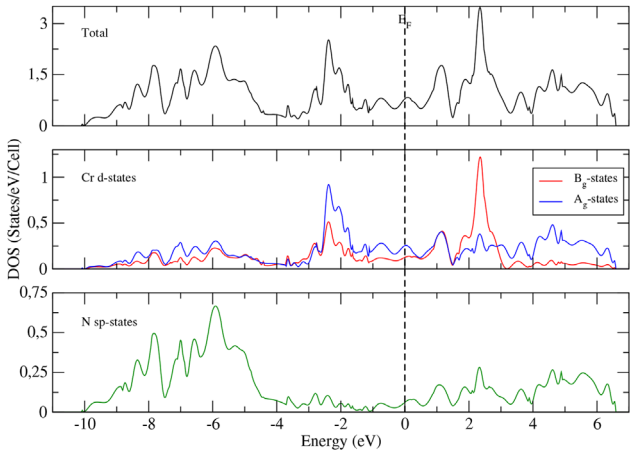

Figure 3. Calculated total and projected DOS for Structure Model 1. DOS was projected on *d* orbitals of chromium and *sp* orbitals of nitrogen.

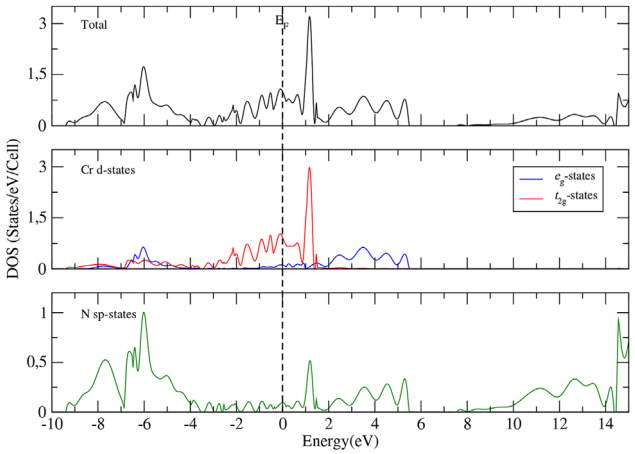

Figure 5. Calculated total and site projected DOS on Cr and N for Structure Model 2.

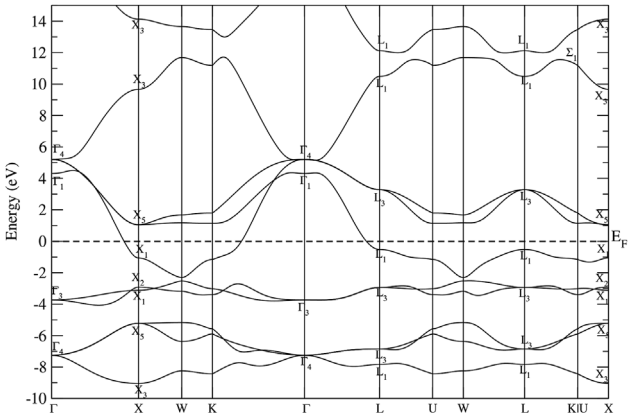

Figure 6. Calculated dispersion relation for Structure Model 3. The dispersion relation is labeled in the same way as **Figure 4**.

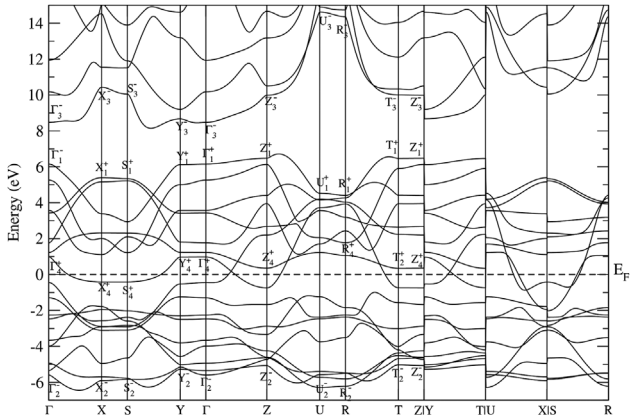

Figure 8. Calculated dispersion relation for Structure Model 4. All labels refer to 1-dimensional irreps.

The Cr atom is in a site with point group symmetry C_{2h}, and according to the splitting of the crystal field, the *d*-type states of Cr split into three nondegenerate A_g and two nondegenerate B_g states, whose contributions to total DOS can be seen in Figure 3. The N *p* states are dominant in the first six bands, with a contribution of ≈60%, as indicated by the odd representations appearing in the first two bands of Figure 2. Bands near E_F (from −4 eV until 4 eV) are constituted mainly by *d*-type states with a mixture of A_g and B_g states. The former constitutes almost entirely (with contributions of ≈70%) the two bands crossing E_F, and the latter is dominant near the 2 eV eigenvalue, with a 60% contribution. The irreps corresponding to the labels of bands in this energy range transform as chromium *d*-states.

Given the low symmetry of the structure, it exhibits few irreps, which are mostly 1-dimensional, and as a consequence, many level anticrossings appear in the dispersion relation, as can be seen in Figure 2. Above 4 eV, the bands are constituted by a mixture of N *sp*-type states and A_g, similar to the situation that happens in the first six bands. Unlike these first bands, in the range above 4 eV, the contribution of A_g states is slightly greater than that of N states. This can be seen, given the even irreps appearing in the last band of the region. This mixture of N and Cr states suggests that the bonds between these atoms are constituted mainly by *sp*-type states and A_g states.

3.2.2. Structure Model 2

The band structure of Structure Model 2 is shown in Figure 4. The lower band region has both the lowest and highest points in the L position, with symmetry D_{3d}, which are separated by an energy width of $\left(E_{L_2^-} - E_{L_1^+}\right) = 15.13$ eV. The upper region has its lowest point at the Γ **k**-point, with symmetry O_h corresponding to the 1-dimensional irrep Γ_1^+, the gap between these two regions is 1.72 eV. Because of the crossing of the energy bands with E_F this phase of CrN is an electric conductor. This agrees with the experimental reports for the electronic behavior in the NaCl-type phase.[10] The dispersion relation for this crystal is similar to previously reported works.[10,25]

Figure 5 shows the DOS in the same energy interval in which the dispersion relation was calculated. As can be seen, there are

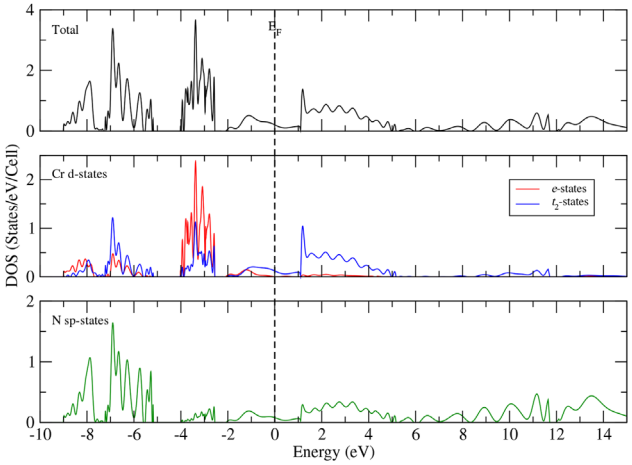

Figure 7. Calculated total and site projected DOS on Cr and N for Structure Model 3.

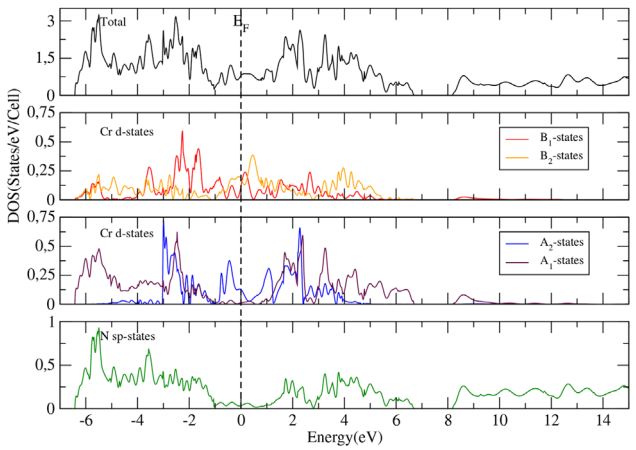

Figure 9. Calculated total and site projected DOS on Cr and N for Structure Model 4.

states at E_F that confirm the conducting behavior of Structure Model 2. Exactly as in Structure Model 1 total DOS shows a maximum at E_F indicating an instability or an spin population splitting. Table 2 shows that either Cr and N have point group symmetry O_h and following the splitting of the crystal field, the *d*-type states of Cr split into one e_g twofold degenerate state and a t_{2g} threefold degenerate states. The N states now transform as t_{1u} states, which are dominant in the three first bands shown in Figure 4 that contribute with 88, 72, and 58%, respectively. These states transform as the odd irreps that label these three bands. The next set of three bands that form a threefold degenerate eigenvalue at Γ are constituted mainly by t_{2g} states with almost 90% of the contribution, which agrees with previous works.[25,48] There is also another pair of bands that join at Γ point that are composed mainly of e_g states with proportions of 72 and 66%. These five bands have the symmetry of even irreps that transform as *d* states. The region separated by the gap is only composed by *s* nitrogen states, as indicated by the even 1-dimensional irreps that label the first band of this region. Bands constituted mainly by e_g states seem to have a considerable contribution of t_{1u} states and conversely. This indicates a strong coupling between these states, which means that bonding and antibonding states in this phase are composed only of e_g and nitrogen states, leaving t_{2g} states as nonbonding.[21]

3.2.3. Structure Model 3

The band structure of Structure Model 3 is shown in **Figure 6**. It is easy to see that this phase is an electric conductor since the Fermi level crosses some bands. This dispersion relation is constituted by four band regions that do not overlap. The lowest one has a width of 3.88 eV. This region is separated from the upper one by 1.10 eV (which has a 1.55 eV width) and is separated from the central region by 0.21 eV. The central band region has a width of 14.02 eV and is separated from the region above by 0.26 eV.

Figure 7 shows the total and projected DOS for the energy interval of the dispersion relation. In the total DOS can be seen the corresponding gaps between regions. The crystal field splits the *d*-type states of Cr into twofold *e* states and threefold t_2 states, while N *p* states transform like t_2 states, given that the two atoms have symmetry point group T_d. Figure 7 shows the individual contribution of the split *d*-type states of Cr. The first region consisting of three bands that form a triplet at Γ is composed mostly of t_2 states of N contributing with nearly 55%. The next region of two bands is composed mainly of *e* states of chromium, allowing the formation of a twofold eigenvalue at Γ. The contribution of these states is 62% to the first band and of 73& to the second one. At the next region, there are four bands. The contribution of *e* states is small, having a maximum contribution of 13% in the first band and negligible in the next three bands. These bands are a mixture of the t_2 states of Cr and N, whose minimum contribution is 92%.

The highest energy band is composed completely of nitrogen states. In the dispersion relation, it can be seen that no irrep has a defined parity. This is because the point group symmetry T_d does not have the inversion operation and either Cr and N atoms have that symmetry. The first three bands of the region transform mainly as N t_2 states (or as *p* states) but also as Cr states, which contribute with nearly 27%. However these Cr states are *d* states. The inverse situation happens in the next three bands that form a triplet near 6 eV, but this time the *s* states of N also contribute since the lower band transforming as *s* states gets mixed with the triplet in the Δ **k**-line. As a consequence, the states that form bonding and antibonding orbitals are the t_2 states of Cr and the N states *p* and *s*. Then *e* states are nonbonding, which agrees with the analysis of Ref. [21].

3.2.4. Structure Model 4

Figure 8 shows the dispersion relation for Structure Model 4. It can be observed that the structure has a main region that crosses E_F overlapping the valence and conduction regions indicating, that Structure Model 4 is an electric conductor. The lower band region has a width of approximately 13.17 eV and is separated from the upper one by 1.43 eV. From the dispersion relation at the lower region, it can be noted that the structure in some **k**-lines is dispersionless.

As shown in Table 2, Cr atom is in a position with point group symmetry C_{2v} as well as the N atom. For this symmetry, the crystal field theory predicts a splitting into two A_1, one A_2, one B_1, and one B_2 states for Cr; and two A_1, one B_1 and one B_2 states for nitrogen all of them being nondegenerate. The contribution for each Cr state to DOS can be seen in **Figure 9** as well as the projection for the *sp*-type states of N and the total DOS, all of them depicted in the same energy range than in dispersion relation. The first bands are dominated principally by N *p*-type states, as confirmed by the odd irreps in the first band. At E_F, the bands mainly are constituted by the A_2, B_1, and B_2 states of Cr reaching a maximum of contribution of 20% and a minimum of 11% at the two bands crossing E_F. This can be seen in Figure 8 by the even irreps that appear in a band crossing E_F. The other bands are constituted by a mixture of *sp*-type states and two or three *d*-type states, except for the bands belonging to the region above the gap, which are almost entirely (≈70% of contribution) constituted by N states that transform as odd irreps, as can be seen in the dispersion relation, so these are *p* states.

It is interesting that either the N states and A_1 states constitute the highest and the lowest bands of the central region also those states appear to have a correlated behavior since in the upper region the only nonvanishing *d*-type state contribution is that of the A_1 states. This suggests that those states are mainly responsible for the bonds between Cr and N. As in Structure Model 1, this structure has low symmetry and, thus, has few 1-dimensional irreps, inducing many level anticrossings in the electronic band structure.

3.3. Topological Classification of Crystals

The study of topological properties of the electron density in each phase helps determine the ionicity or covalence of the materials presented using the QTAIM analysis[49,50] by the means of a bond critical point (BCP) study. The information about the BCPs for each studied phase is shown in **Table 3**. The list shows that all

Table 3. Properties of BCP for each studied structure model. The values ρ_b and $\nabla^2\rho_b$ are the electron density and the Laplacian of the density, respectively. λ_1, λ_2 and λ_3 are eigenvalues of the hessian matrix. All magnitudes are given in atomic units.

SM	Bond	ρ_b	$\nabla^2\rho_b$	λ_1	λ_2	λ_3	ε
1	Cr—N	0.0919	0.3591	−0.1069	−0.0906	0.5566	0.1799
2	Cr—N	0.0755	0.3315	−0.0677	−0.0677	0.4671	0.0000
3	Cr—N	0.1253	0.4688	−0.1777	−0.1777	0.8241	0.0000
4	Cr—N	0.1838	0.7392	−0.3126	−0.3052	1.3570	0.0242
	$N—N^1$	0.0178	0.0687	−0.0116	−0.0026	0.0829	3.4615
	$N—N^2$	0.0073	0.0342	−0.0058	−0.0038	0.0439	0.5263
	$Cr—Cr^1$	0.0890	0.0998	−0.1369	−0.0931	0.3299	0.4705
	$Cr—Cr^2$	0.0330	0.0265	−0.0260	−0.0232	0.0689	0.1207

present bonds in each structure are ionic since all Laplacians are positive. Table 3 also gives the ellipticity ε, which is defined as $\varepsilon = \lambda_1/\lambda_2 - 1$.

Structure Model 1 has a Cr-N ionic bond that is unlocalized given the deviation of ε from zero. Since ε is equal to zero for the ionic bonds in Structure Models 2 and 3, those are localized and have a cylindrical shape. Structure Model 4 is a special case, given the many kinds of bonds present in this structure. On the one hand, there is an ionic Cr-N bond that is a little unlocalized, given that $\varepsilon \sim 0$. Secondly, there are two different ionic N-N bonds one of which is highly unlocalized since $\varepsilon >> 0$. Finally, there are two ionic bonds between Cr atoms that are unlocalized.

The gradient trajectories and Laplacian contour plots of the electron density obtained with the TOPOND package and the BCPs in the conventional cells are shown in Figure 10–13. The 2D maps were depicted in plane [100] for Structure Models 1 and 2, in plane [110] for Structure Model 3 and in [001] plane for Structure Model 4. These planes were chosen because they contain all the types of bonds present on each phase, except for Structure Model 4, where only one Cr-Cr bond, one N-N bond, and the Cr-N bond were depicted. The graphics also show the boundaries of the atomic basins that intercept the lines connecting atoms in bond or ring critical points indicated by black dots in the contour plots. The black-dashed lines in those plots indicate negative values of the Laplacian.

Figure 10a, 11a, 12a, and 13a show that the Laplacian dashed lines are only in the vicinity of the nuclei forming shells. This indicates that the electron density has local maxims only around the nuclei, which is characteristic of ionic bonding, confirming the previous affirmations about the bonding types.

For Structure Model 1, the topological plots are shown in Figure 10. Figure 10a shows the BCP between the Cr and N atoms, which are also depicted in Figure 10b. The critical point connecting chromiums forming a chain of atoms is a ring critical point (RCP), which is bounded by a ring of atoms. The ring around this RCP lies outside the plane of Figure 10a and cannot be shown.

For Structure Model 2, the topological plots are shown in **Figure 11**. Figure 11a shows that the BCPs are located in a trajectory that links the Cr and N atoms, as can also be seen in Figure 1b. In Figure 11a one can see that between two chromium atoms, there is an RCP that is bounded by those atoms and two N atoms forming the ring.

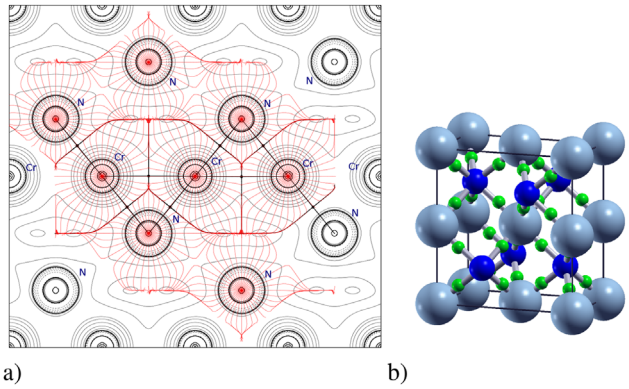

Figure 10. Topology of Structure Model 1. a) Laplacian contour plot and gradient directions in the [100] plane, and (b) bond critical points in the conventional cell. The convention for these images is: small balls indicate a BCP, medium balls represent nitrogen, and big balls represent Cr atoms. For all contour plots, the black-dashed lines indicate a negative Laplacian.

For Structure Model 3, the topological plots are shown in **Figure 12**. In Figure 12a, the concentration between two atoms represent a BCP with every nitrogen atom in the plane bonded with two chromium atoms as can also be seen in Figure 12b. The plane of the Laplacian contour plot only exhibit BCPs not RCPs.

For Structure Model 4 the topological plots are shown in **Figure 13**. In Figure 13a, only one kind of Cr-Cr and N-N bond besides the Cr-N one are shown. The missing bonds can be seen in Figure 13b. There are two critical points between N atoms; the one that lies in a longer line is a BCP, while the other is an RCP surrounded by four Cr and two N forming an asymmetric hexagon. The same situation happens for Cr, but this time the critical point lying in the shorter line linking two Cr atoms is a BCP and the other is an RCP that is bounded by four nitrogens and two chromiums, forming an asymmetric hexagon. It is interesting to note that the {001} planes are highly connected capes that are bonded to one another by the Cr-Cr and N-N bonds missing on those planes, and thus forming a layered structure.

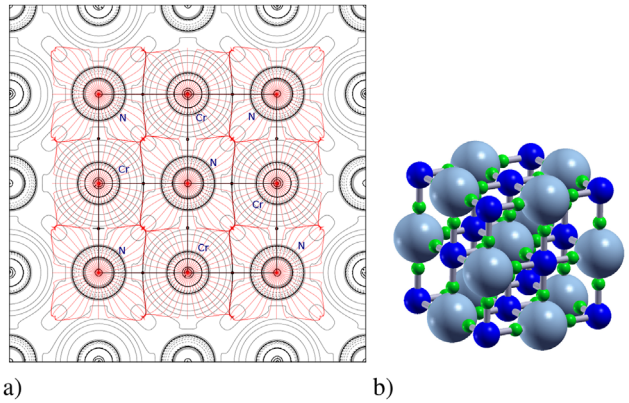

Figure 11. Topology of Structure Model 2. a) Laplacian contour plot and gradient directions in the [100] plane, (b) BCP in the conventional cell.

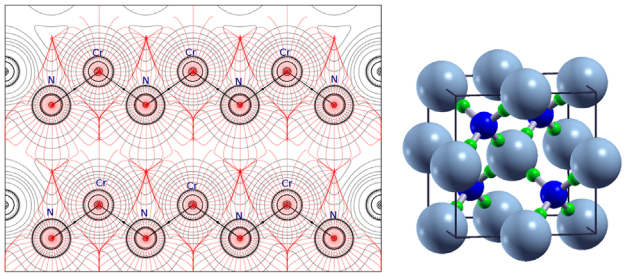

Figure 12. Topology of Structure Model 3. a) Laplacian contour plot and gradient directions in the [110] plane, (b) BCP in the conventional cell.

As a final comment is important to note that each Structure Model presents conducting behavior even though every bond is ionic. Given that these calculations were made without any magnetic ordering it is not expected that a gap opens at E_F as said in previous reports[10] and these untypical observations appear. As said before is mandatory to do some dynamic stability research on these structures to confirm these apparent contradictions or discard them. Nonetheless is more likely that imposing magnetic ordering would lead to a gap opening at E_F and therefore the structures would be non-conducting.

4. Conclusions

In the present work, DFT calculations with hybrid functionals (Hartree-Fock + GGA) and Gaussian basis sets have been used in order to study four crystal phases of CrN. Two of them are hypothetical with space group *Cmcm* and *Pmmm*, and the other two have been reported experimentally (NaCl-type, space group $Fm\bar{3}m$) and theoretically (zinc-blende-type, space group $F\bar{4}3m$). The calculated lattice parameters of reported structures are in good agreement with previous researches (1.8 and 0.86% of error, respectively). The methods used to calculate those quantities were applied to the hypothetical phases, and a structural description of them was possible. The calculation of the cohesive energy for each crystal made it possible to determine that every structure is thermodynamically stable.

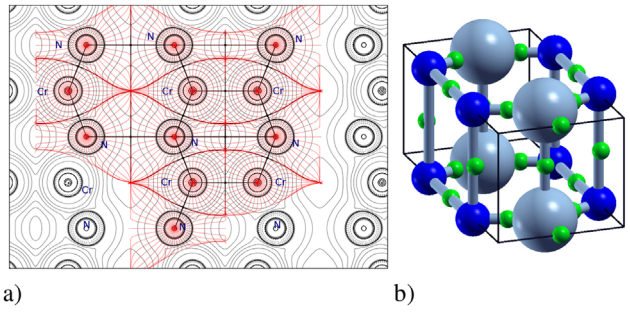

Figure 1 3. Topology of Structure Model 4. a) Laplacian contour plot and gradient directions in the [001] plane, and (b) BCP in the conventional cell.

Our calculations yielded that the nonsynthesized structure *Cmcm* was the most stable among the studied phases. However, it seems not to be much more stable than the experimental NaCl-type structure, since the difference between E_{coh} is only 0.35 eV. More studies on this orthorhombic phase are to be made in order to confirm or discard its relative stability, for example, the calculation of phonon dispersion in order to determine its dynamic stability or calculation of elastic constants to evaluate the Born criteria of mechanical stability.

Using the same DFT methods, electronic dispersion relation and density of electronic states were calculated. The results show that each studied phase is a conductive one and also that this work is in agreement with previous reports of electronic structure about NaCl-type and zinc-blende-type phases. Not only the form but also the compositions of the bands have been accurately determined. In addition, the decomposition of the Cr *d* states in the DOS graphics was determined. With aid of bond critical points, this study was able to provide a description of the bonding structure for each phase to conclude that all bonds in all structures are ionic. Also, the topology of the electron density and the theory of atoms in molecules (QTAIM) allowed for the identification of RCPs in Laplacian contour plots.

It is interesting to note that the NaCl-type phase is an ionic crystal because of its topology and that is also a good conductor given that the crystal field splits the chromium *d* states into two states, one of which is nonbonding and mainly constitutes bands at the Fermi level. On the contrary, the zinc-blende phase does not seem to be a good conductor. Here the crystal field also splits chromium *d* states into two states, but this time the nonbonding states do not contribute so much to E_F, which is entirely constituted by bonding states. As a consequence, the DOS at this level is very low.

One also should expect the *Cmcm* phase to be a bad conductor since the bonding states are dominant at the Fermi level. However there is also a non-negligible contribution of the nonbonding states that could contribute to a higher electron mobility. Regarding the highly bonded *Pmmm* structure, the crystal field splits the Cr *d* states into four different states, the bonding states (between Cr and N) have a negligible contribution to E_F, suggesting that this material could have a good electron mobility. Additionally, there are other kinds of bonds, and the other "nonbonding" states should form these Cr-Cr and N-N bonds. These states almost totally constitute the Fermi level having as a consequence that the electron mobility and also the conductivity is reduces. The reproduction of the electronic structure presented in previous works for the reported structures is an indicator of the validity of the use of the hybrid B3LYP functional for calculations with structures of CrN.

Acknowledgments

This work was supported by Universidad EAFIT – COLCIENCIAS under Grant No. 0479-2013, Code 30409. In addition, the authors would like to thank Universidad EAFIT and COLCIENCIAS for funding the Project 767-000060 "Propiedades estructurales, mecánicas y magnéticas de nuevas fases hipotéticas del CrN". Thanks also to Prof. Alejandro Strachan and Mathew Cherukara (Purdue University) for their helpful discussions and feedback and to the Centro de Computación Científica Apolo – Universidad EAFIT for computing facilities.

Conflict of Interest

The authors declare no conflict of interest.

Keywords

B3LYP functional, chromium nitride, density functional theory, electronic structure, topology

Received: August 8, 2017
Revised: October 4, 2017
Published online: November 7, 2017

[1] P. Panjan, B. Navinšek, A. Cvelbar, A. Zalar, I. Milošev, *Thin Solid Films* **1996**, *281–282*, 298.
[2] P. Hones, C. Zakri, P. E. Schmid, F. Lévy, O. R. Shojaei, *Appl. Phys. Lett*. **2000**, *76*, 3194.
[3] L. E. Toth, *Transition Metal Carbides and Nitrides*, Academic Press, New York **1971**.
[4] J. Stockemer, R. Winand, P. V. Brande, *Surf. Coat. Technol*. **1999**, *115*, 230.
[5] C. P. Constable, J. Yarwood, P. Hovsepian, L. A. Donohue, D. B. Lewis, W. D. Münz, *J. Vacuum Sci. Technol. A* **2000**, *18*, 1681.
[6] B. Eck, R. Dronskowski, M. Takahashi, S. Kikkawa, *J. Mater. Chem*. **1999**, *9*, 1527.
[7] X. Y. Zhang, J. S. Chawla, B. M. Howe, D. Gall, *Phys. Rev. B* **2011**, *83*, 165205.
[8] L. He, Z. Zhi, *Chin. Phys. B* **2011**, *20*, 077102.
[9] Y. Liang, X. Yuan, W. Zhang, *Solid State Commun*. **2010**, *150*, 2045.
[10] A. Herwadkar, W. R. L. Lambrecht, *Phys. Rev. B* **2009**, *79*, 035125.
[11] M. N. Eddine, E. F. Bertaut, M. Roubin, J. Paris, *Acta Crystallogr. B* **1977**, *33*, 3010.
[12] L. M. Corliss, N. Elliott, J. M. Hastings, *Phys. Rev*. **1960**, *117*, 929.
[13] N. Shulumba, B. Alling, O. Hellman, E. Mozafari, P. Steneteg, M. Odén, I. A. Abrikosov, *Phys. Rev. B* **2014**, *89*, 174108.
[14] F. Rivadulla, M. Banobre-Lopez, C. X. Quintela, A. Pineiro, V. Pardo, D. Baldomir, M. A. Lopez-Quintela, J. Rivas, C. A. Ramos, H. Salva, J. Zhou, J. B. Goodenough, *Nature Mater*. **2009**, *8*, 947.
[15] A. Björn, T. Marten, I. A. Abrikosov, *Nature Mater*. **2010**, *9*, 283.
[16] X. Y. Zhang, D. Gall, *Phys. Rev. B* **2010**, *82*, 045116.
[17] L. Zhou, F. Körmann, D. Holec, M. Bartosik, B. Grabowski, J. Neugebauer, P. H. Mayrhofer, *Phys. Rev. B* **2014**, *90*, 184102.
[18] A. S. Botana, F. Tran, V. Pardo, D. Baldomir, P. Blaha, *Phys. Rev. B* **2012**, *85*, 235118.
[19] M. Marín-Suárez, M. E. Vélez, J. David, M. Arroyave-Franco, *Comput. Mater. Sci*. **2016**, *122*, 240.
[20] V. Antonov, I. Iordanova, *J. Phys.: Conf. Series* **2010**, *223*, 012043.
[21] M. S. Miao, W. R. L. Lambrecht, *Phys. Rev. B* **2005**, *71*, 214405.
[22] A. Filippetti, W. E. Pickett, B. M. Klein, *Phys. Rev. B* **1999**, *59*, 7043.
[23] A. Filippetti, N. A. Hill, *Phys. Rev. Lett*. **2000**, *85*, 5166.
[24] B. Alling, T. Marten, I. A. Abrikosov, *Phys. Rev. B* **2010**, *82*, 184430.
[25] M. Brik, C. G. Ma, *Comput. Mater. Sci*. **2012**, *51*, 380.
[26] K. B. Wiberg, R. F. W. Bader, C. D. H. Lau, *J. Am. Chem. Soc*. **1987**, *109*, 985.
[27] R. F. W. Bader, P. L. A. Popelier, T. A. Keith, *Angew. Chem*. **1994**, *106*, 647.
[28] P. F. Zou, R. F. W. Bader, *Acta Crystallogr. A* **1994**, *50*, 714.
[29] R. F. W. Bader, *J. Phys. Chem. A* **1998**, *102*, 7314.
[30] R. Dovesi, V. R. Saunders, R. Roetti, R. Orlando, C. M. Zicovich-Wilson, F. Pascale, B. Civalleri, K. Doll, N. M. Harrison, I. J. Bush, P. D'Arco, M. Llunell, CRYSTAL09 User's Manual University of Torino Torino, URL, **2009**.
[31] R. Dovesi, R. Orlando, B. Civalleri, C. Roetti, V. R. Saunders, C. M. Zicovich-Wilson, *Zeitschrift für Kristallographie* **2005**, *220*, 571.
[32] A. R. Oganov, C. W. Glass, *J. Chem. Phys*. **2006**, *124*, 244704.
[33] C. W. Glass, A. R. Oganov, N. Hansen, *Computer Phys. Commun*. **2006**, *175*, 713.
[34] A. R. Oganov, A. O. Lyakhov, M. Valle, *Acc. Chem. Res*. **2011**, *44*, 227.
[35] P. Hohenberg, W. Kohn, *Phys. Rev*. **1964**, *136*, B364.
[36] W. Kohn, L. J. Sham, *Phys. Rev*. **1965**, *140*, A1134.
[37] R. O. Jones, O. Gunnarsson, *Rev. Mod. Phys*. **1989**, *61*, 689.
[38] A. D. Becke, *J. Chem. Phys*. **1993**, *98*, 5648.
[39] S. H. Vosko, L. Wilk, M. Nusair, *Can. J. Phys*. **1980**, *58*, 1200.
[40] C. Lee, W. Yang, R. G. Parr, *Phys. Rev. B* **1988**, *37*, 785.
[41] M. Towler, CRYSTAL reosurces page.
[42] H. J. Monkhorst, J. D. Pack, *Phys. Rev. B* **1976**, *13*, 5189.
[43] W. Setyawan, S. Curtarolo, *Comput. Mater. Sci*. **2010**, *49*, 299.
[44] M. I. Aroyo, D. Orobengoa, G. de la Flor, E. S. Tasci, J. M. Perez-Mato, H. Wondratschek, *Acta Crystallogr. A* **2014**, *70*, 126.
[45] C. Gatti, *TOPOND: An Electron Density Topological Program for Systems Periodic (N = 0-3) Dimensions. User's Manual*, CNR-ISTM, Milano **1999**.
[46] A. Kokalj, *Comput. Mater. Sci*. **2003**, *28*, 155.
[47] C. Kittel, *Introduction to Solid State Physics*, 8th ed., John Wiley and Sons, Hoboken, NJ **2008**.
[48] D. A. Papaconstantopoulos, W. E. Pickett, B. M. Klein, L. L. Boyer, *Phys. Rev. B* **1985**, *31*, 752.
[49] V. Luana, M. A. Blanco, A. Costales, P. Mori-Sánchez, A. M. Pendás, *Topology and Properties of the Electron Density in Solids: The Quantum Theory of Atoms in Molecules*. WILEY-VCH, Weinheim, Germany **2007**.
[50] C. F. Matta, R. J. Boyd, *The Quantum Theory of Atoms in Molecules*. Wiley-VCH, Weinheim, Germany **2007**.